International Journal of Engineering, Mathematical and Physical Sciences
ISSN: 2517-9934
Vol:5, No:1, 2011

Neutron Flux Characterization for Radioisotope Production at ETRR-2

A. M. Hassanain, Nader M. A. Mohamed, M. Naguib Aly, Alya A. Badawi and M. A. Gaheen

***Abstract*—**The thermal, epithermal and fast fluxes were calculated for three irradiation channels at Egypt Second Research Reactor (ETRR-2) using CITVAP code. The validity of the calculations was verified by experimental measurements. There are some deviations between measurements and calculations. This is due to approximations in the calculation models used, homogenization of regions, condensation of energy groups and uncertainty in nuclear data used. Neutron flux data for the three irradiation channels are now available. This would enable predicting the irradiation conditions needed for future radioisotope production.

***Keywords*—**ETRR-2, Neutron flux, Radioisotope production, CITVAP

I. Introduction

ETRR-2 is a multi-purpose open pool type reactor with a nominal power of 22 MW. The reactor core is cooled and moderated by dematerialized water and reflected by beryllium blocks [1]. The design concept is based on the requirement of being a reactor of versatile utilization. The ETRR-2 reactor has been designed mainly for radioisotope production [2]. The extent of the utilization of the reactor is basically determined by its power level, which in turn determines the neutron flux available, as well as its operational schedule. Factors that determine the type of nuclear reaction taking place and the production rate of the radioisotope are [3]: energy of the neutrons and the neutron flux, characteristics of the target material and activation cross-section for the desired reaction. Therefore, it is necessary to characterize the neutron flux in positions used for radioisotope production in the reactor to evaluate the radioisotopes yields. The resulting flux data will be a guide for radioisotope production program. In this paper the results of the calculations are presented. The validity of these calculations is verified by experimental measurements which were done early by the authors [4]. The calculations were carried out at the same control rods positions of experiment state which was 45% extraction out of the core for control rods no. 1, 2, 4 and 6, while control rods no. 3 and 5 were used as safety rods "100% extraction".

A. M. Hassanain is with Egypt Second Research Reactor, The Atomic Energy Authority of Egypt.
N. M. A. Mohamed is with Egypt Second Research Reactor, The Atomic Energy Authority of Egypt (Email: nmohamed@ictp.it).
M. Naguib Aly is with Nuclear and Radiation Engineering Department, Alexandria University, Alexandria, Egypt
Alya A. Badawi is with Nuclear and Radiation Engineering Department, Alexandria University, Alexandria, Egypt
M. A. Gaheen is with Egypt Second Research Reactor, The Atomic Energy Authority of Egypt.

II. Methodology

For the cell calculation, WIMSD-4 code [5] was used, which has its own nuclear data library, with the collision probability option in one dimensional geometry (slab) and 69 neutron energy groups. POS-WIMS code [6] was used between cell calculation and core calculation to make second homogenization and get library cross sections in core codes format. CITVAP code [7] was used to perform core calculations in the x-y-z geometry and to follow up the loading of fuel in all loading cycles. In the present work, the core is divided into twenty axial segments of 4 cm each. Two layers with 20 cm of water were added above and below the active length of the core (80cm). The total length of the core model is 120 cm. The final dimensions of the core are (120 x 97 x 120) cm. The neutronic core calculations were carried out for all core cycles (from first core to the present sixth core). Axial thermal, epithermal per unit lethargy and fast flux distributions for the three irradiation channels are calculated with input options approximate to conditions of the experiment but at full power of 22 MW.

III. Results And Discussion

The results of the calculations are plotted in figures from 1 to 17. The measured values [4] of thermal flux and epithermal flux for every channel are plotted on the corresponding chart of calculated flux distributions for comparison. There are some deviations between measurements and calculations. This is due to approximations in the calculation models used, homogenization of regions, condensation of energy groups and uncertainty in nuclear data used.

A. Thermal Neutron Flux

The calculated and the measured flux distributions have the same trend (figures 1, 2 and 3). However, there is a shift in calculated flux to up with respect to the core. This is because of the effect of the control rods on thermal neutron flux is more pronounced in measurements than calculations. For the irradiation channels G3 and H10, the thermal flux in the north side is greater than it in the south side (figures 4 and 6). This is due to the effect of surrounding materials in the neighboring channel on thermalization into the irradiation channel. For the irradiation channel E3, it is clear that the north and south sides have approximately the same thermal flux distributions (figure 5).

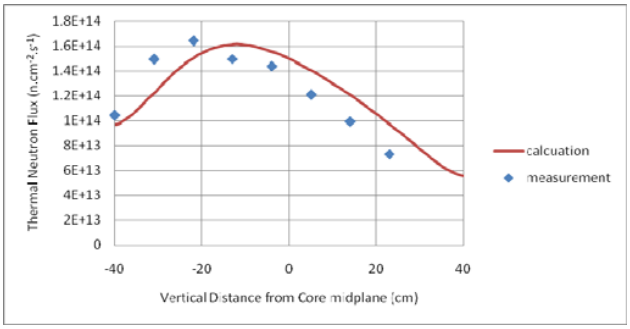

Fig. 1 Calculated and Measured axial thermal neutron flux distributions for irradiation channel G3 – South side.

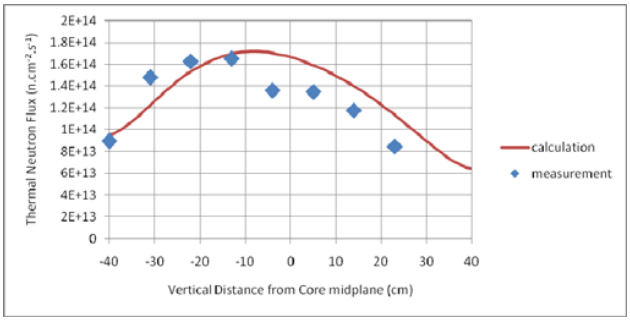

Fig. 2 Calculated and Measured axial thermal neutron flux distributions for irradiation channel E3 – South side.

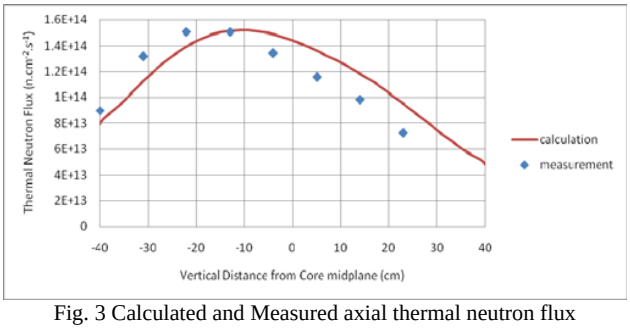

Fig. 3 Calculated and Measured axial thermal neutron flux distributions for irradiation channel H10 – North side.

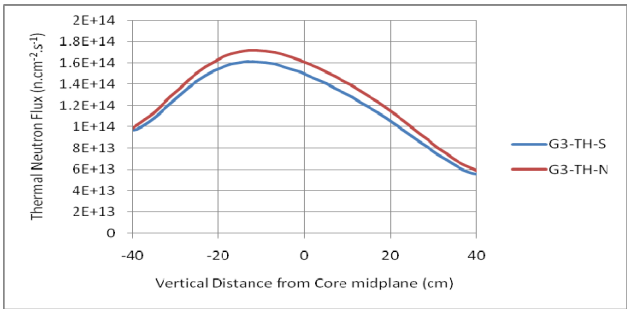

Fig. 4 Calculated axial thermal neutron flux for irradiation channel G3 – South and North sides

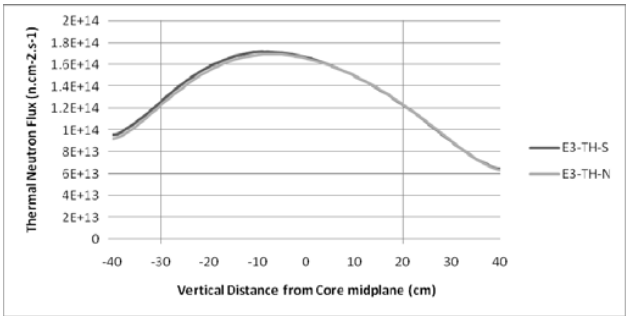

Fig. 5 Calculated axial thermal neutron flux distributions for irradiation channel E3 – South and North sides.

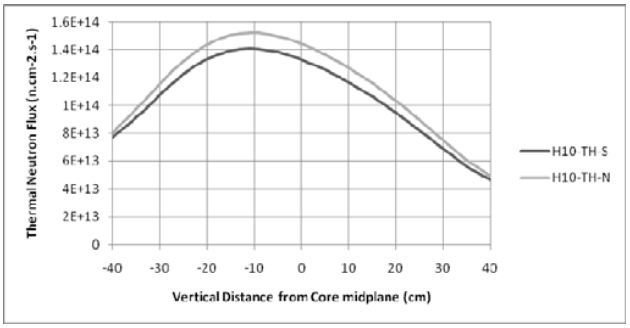

Fig. 6 Calculated axial thermal neutron flux distributions for irradiation channel H10 – South and North sides.

B. Epithermal Neutron Flux

The calculated and measured axial epithermal neutron flux distributions for south side of irradiation channel G3, E3 and H10 are shown in figures 7, 8 and 9, respectively. It is clear in the figures that the calculated and measured flux distributions have the same trend in the lower shelves in the irradiation channel. However, there is a significant excess in the calculated epithermal flux values in the shelves in the irradiation channel. Those upper shelves which are adjacent to the control rods positions at the time of experiment. The effect of control rods on the epithermal neutron flux doesn't appear in a clear way in the calculation.

The calculated axial epithermal neutron flux distribution for South and North sides of irradiation channels G3 and E3 are shown in figures 10 and 11 respectively. The north and south sides have approximately the same epithermal flux distributions. Values of epithermal neutron flux in both sides are nearly the same. For the irradiation channel H10, it is clear that epithermal flux in the south side is greater than it in the north side (figure 12). This is due to the difference in thermalization effect between the two sides.

C. Fast Neutron Flux

The calculated axial fast neutron flux distributions for South and North sides of irradiation channels G3, E3 and H10 are shown in figures 13, 14 and 15 respectively. The fast fluxes at the north and the south sides have approximately the same distributions and values.

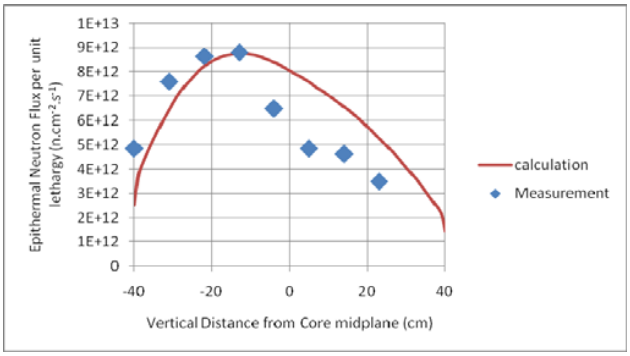

Fig. 7 Calculated and Measured axial epithermal neutron flux distributions for irradiation channel G3 – South side.

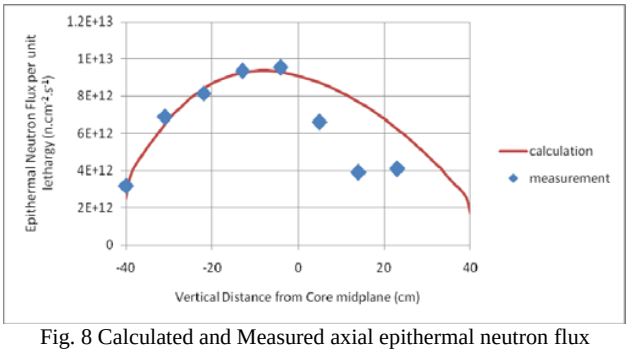

Fig. 8 Calculated and Measured axial epithermal neutron flux distributions for irradiation channel E3 – South side.

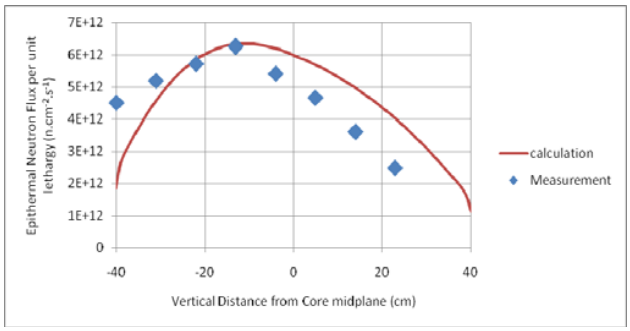

Fig. 9 Calculated and Measured axial epithermal neutron flux distributions for irradiation channel H10 – North side.

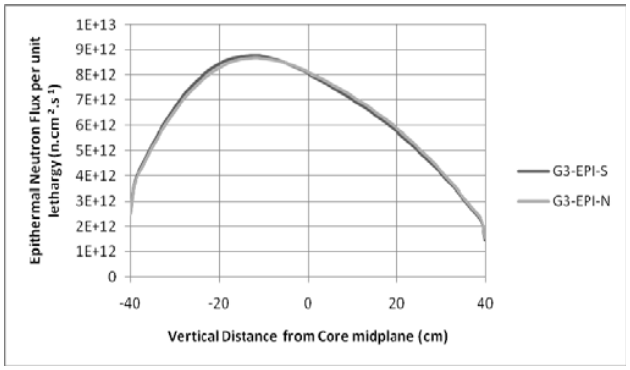

Fig. 10 Calculated axial epithermal neutron flux distributions for irradiation channel G3 – South and North sides.

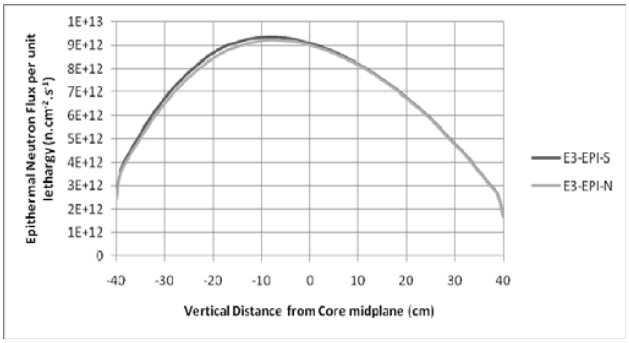

Fig. 11 Calculated axial epithermal neutron flux distributions for irradiation channel E3 – South and North sides

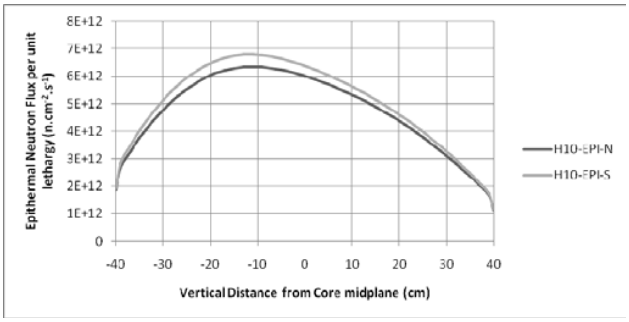

Fig.12 Calculated axial epithermal neutron flux distributions for irradiation channel H10 – South and North sides

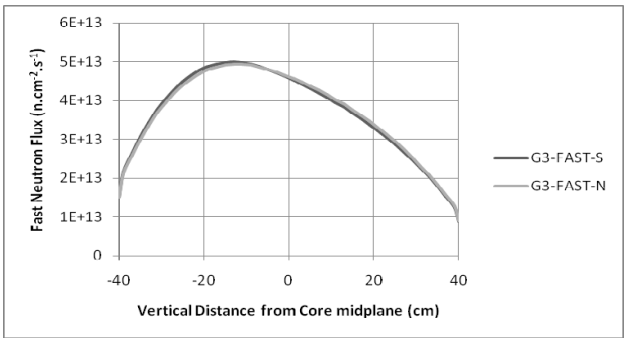

Fig. 13 Calculated axial fast neutron flux distributions for irradiation channel G3 – South and North sides.

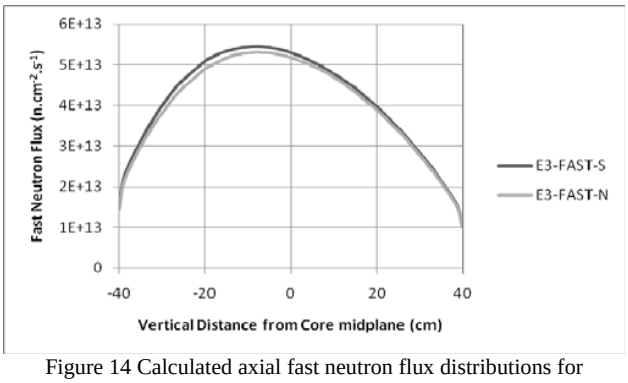

Figure 14 Calculated axial fast neutron flux distributions for irradiation channel E3 – South and North sides.

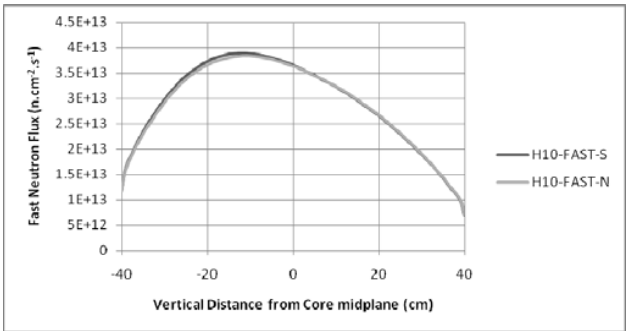

Fig. 15 Calculated axial fast neutron flux distributions for irradiation channel H10– South and North sides.

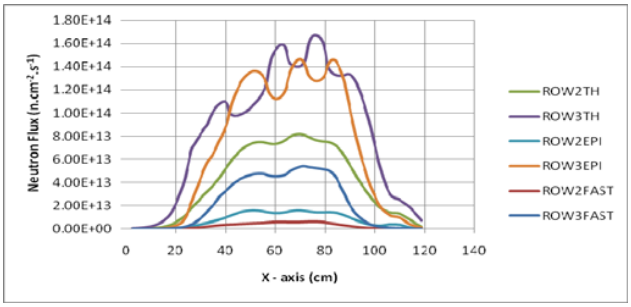

Fig.16 Distributions of calculated maximum Thermal, Epithermal, and Fast fluxes along row 2 and 3.

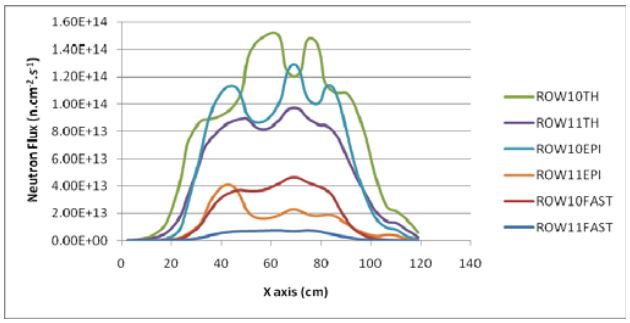

Fig. 17 Distributions of calculated maximum Thermal, Epithermal, and Fast fluxes along row 10 and 11.

D.Maximum Flux in the irradiation channels

Maximum thermal, epithermal and fast flux values have been estimated at the middle of the reactor cycle for each couple of rows that include the irradiation channels surrounding the core in its both sides. Namely, rows numbers: 2 and 3 for one side, and 10 and 11 for the other side. The calculations were done at 50% extraction out of the core for control rods no. 1, 2, 4 and 6, while control rods no. 3 and 5 were safety rods "100% extraction". The distributions of calculated maximum thermal, epithermal, and fast fluxes along row 2 and 3 are plotted in figure 16. It can be emphasized from the figure, that there is a considerable difference in the values among thermal, epithermal and fast fluxes on the same row. Also, there is a large drop in the flux values in the row 2 comparing to those of row 3 which is close to the core.

The successive peaks in thermal flux values for the row closed to the core (row 3) exist at the irradiation channels and in the distance between them where the boxes of the core reflectors are located. On the other hand, the successive peaks in epithermal flux values for row 2 exist at the channels where the core reflectors are located. The distributions of calculated maximum Thermal, Epithermal, and Fast fluxes along row 10 and 11 are plotted in figure 17. There is a considerable difference in the values among thermal, epithermal and fast fluxes on the same row. Also, there is a large drop in the flux values in the row 11 comparing to those of row 10 which is close to the core.

IV. CONCLUSIONS

Thermal, epithermal and fast axial flux distributions were calculated for the irradiation channels G3, E3 and H10 in ETRR-2. There are considerable variations in thermal flux values in the same irradiation channel. These variations will lead to different activity values for the same type of produced radioisotope. The thermal, epithermal and fast flux distributions for the three irradiation channels have peaks shifted to the lower part of the core in reverse to control rods movement direction. The variation in flux with position can be mainly due to: (1) the relative position to the core, (2) the insertion percentage of control rods adjacent to the irradiation channel, (3) the vertical distance from core mid-plane, (4) the surrounding materials around the irradiation channel, and (5)the Percentage of fuel burn-up in the neighboring of irradiation channel.

The validity of the calculations was verified by a comparison with the experimental values. The comparison shows that there are some differences between calculation and measurement in the upper shelves of sample holders. Uncertainties in calculations are due to approximations in the calculation models used, homogenization of regions, condensation of energy groups and uncertainty in nuclear data used. Neutron flux data for the three irradiation channels are now available. This would enable predicting the irradiation conditions needed for future radioisotope production.

ACKNOWLEDGMENT

The authors wish to thank Prof. Dr. Esmat Amin, Atomic Energy Authority, Egypt.

REFERENCES

[1] O. Villarino, E., 1993. Initial Report Database. 0767 0700-3TANU-135-2A.ETRR-2 Detailed Engineering.
[2] INVAP SE, 1997. Safety Analysis Report of the MPR Reactor,Argentina, 0767-5325- 3IBLI 001-1O.
[3] Manual Of Radioisotope Production, International Atomic Energy Agency, Vienna, 2003.
[4] A. M. Hassanain , Nader M. A. Mohamed , M. Naguib Ali , Alya A.Badawi and M. A. Gaheen, "Measurements of thermal and epithermal neutron fluxes for Radioisotopes production at Research

Reactors",Proceedings of the 1st International Nuclear and Renewable Energy Conference (INREC10), Amman, Jordan, March 21-24, 2010.
[5] Askew, J.R., 1966. A General Description of the Lattice Code WIMS, pp. 564–589, JBNES7.
[6] INVAP SE, 1993. POS-WIMS. MTR-PC User Manual, Argentina.
[7] INVAP SE, 1995. CITVAP3.1. MTR-PC User Manual, Argentina.